

Monte Carlo Simulations of a Median-filter Technique to Discriminate between Particle and Fluid Velocity Fields

I.J. Saridakis¹, T.C.W. Lau¹, L. Djenidi² and G.J. Nathan¹

¹Centre for Energy Technology, School of Mechanical Engineering
University of Adelaide, South Australia 5005, Australia

²School of Engineering
University of Newcastle, New South Wales 2308, Australia

Abstract

An error analysis is reported of a method to discriminate between the tracer particles used to mark the carrier-phase and the suspended particles in a two-phase flow for particle image velocimetry. The discrimination was obtained through application of a median-filter to two-phase image pairs, generated artificially by a Monte Carlo simulation. A Lamb–Oseen vortex was selected as the simulated flow for both the gas- and solid-phases, as it provides a range of velocities within the simulated field. The rotational velocities of both phases were selected to be different, allowing a range of slip velocities to be analysed. Simulations were executed with a range of particle and tracer volumetric loadings, particle sizes and filter widths. This analysis provides much more detail than was previously available on the conditions for which a median filter will accurately discriminate between tracers and larger particles in a real flow.

Introduction

Particle-laden flows are an important class of flow due to their significance in industrial processes, such as pulverised coal combustion. Modelling of such flows is difficult, due to inter-phase interactions and the difference in the behaviour of the fluid and particle phases. Knowledge of the separate velocity fields of the fluid and particle phases is important to advance understanding of the inter-phase interactions in particle-laden flows. However, the discrimination between the large particle and fluid (marked by small tracer particles) phases is challenging using particle image velocimetry (PIV), since the signal from both phases is superimposed on the same image. Hence their signals must be separated to allow their velocity fields to be determined independently.

A range of techniques have previously been used to discriminate between phases in various two-phase flows [2]. However, most techniques discrimination have utilised a small field-of-view (FOV) – due to a need for high resolution – which mitigates against the simultaneous resolution of large-scale structures. Secondly, most techniques have been applied to flows with low volumetric loading (ϕ_v) so their effectiveness in higher ϕ_v flows is unknown. Consequently, the systematic assessment of a technique that can accurately discriminate between particle and tracer fields for a large range of conditions (ϕ_v , FOV, particle sizes etc.) is required.

Phase discrimination by a median filter is a computationally cheap technique (compared with other techniques) which removes the signal from tracer particles by treating this as high frequency noise, on the basis that the tracer particles are smaller than the typical pixel-size in the image. The tracer-only image is then obtained by subtracting the filtered (particle-only) image from the raw image. Kiger & Pan (1999, 2000) have used a median filter technique, along with a Gaussian mask, to identify

particle locations for particle tracking velocimetry (PTV) [3, 4]. They produced artificial images to optimise the filter kernel size for 4 different groups of particles sizes. Their results suggest that a filter kernel width of 5-7 pixels produces the smallest error and that the particle size has no impact on the error above a critical particle-to-tracer diameter ratio of 3. However, such analysis of the effectiveness of the median filter discrimination technique has yet to be extended to images with higher ϕ_v . In particular, the accuracy of the median filter technique in discriminating between particles and tracers has not been thoroughly investigated for densely seeded two-phase flows.

The aim of the present investigation is therefore to assess systematically the influence of the underlying parameters in a two-phase flow PIV measurement with a median filter phase discrimination technique. Specifically, it aims to assess the separate influences of tracer and large particle ϕ_v , image resolution, filter width and the effect of using polydispersed particles, through Monte Carlo simulation of artificial two-phase images of a vortex flow.

Method

The Monte Carlo method generates a data set by randomly varying one parameter whilst defining the remaining parameters. Here this method was used to generate artificial two-phase images with random distributions of simulated large particles and tracers but with specified properties of the large particle and tracer signals, and of the flow.

A Lamb-Oseen vortex flow was selected to generate the relative translation of each second image in a PIV image pair, because it provides a range of velocities through the image whilst also providing a realistic flow. The velocity in the circumferential direction (V_θ) is given by Equation 1 [6],

$$\frac{V_\theta}{V_{\theta_{max}}} = \frac{R_{max}}{r} \left(1 + \frac{1}{2a}\right) \left[1 - e^{-a\left(\frac{r}{R_{max}}\right)^2}\right] \quad (1)$$

where $V_{\theta_{max}}$ is the peak tangential velocity, $R_{max} = a\sqrt{4\nu dt}$ is the radius at which $V_{\theta_{max}}$ is obtained, r = radial distance (pixels) from vortex centre, ν is kinematic viscosity and the constant $a = 1.25643$ [1]. The radial velocity is zero everywhere.

Each simulation produces both a tracer image pair and a particle image pair, based on simulated Mie scattering. Particle and tracer properties were matched as closely as possible to real particles from previous studies in our lab [5] and are given in Table 1.

Number of particles (N_p)	180
Number of tracers	3000
Tracer diameter	0.05 pix
Median filter width (f)	3 pix
Particle diameter std deviation (as % of mean)	10%
Tracer diameter std deviation (as % of mean)	50%
Image size	300pix \times 300pix
Laser sheet thickness (as % of image size)	2%
Tracer peak tangential velocity ($V_{\theta max}_t$)	8 pix/s
Particle peak tangential velocity ($V_{\theta max}_p$)	11 pix/s
Time separation of image pairs (dt)	1 sec
Interrogation window size (particle image)	32 \times 32
Interrogation window size (tracer image)	24 \times 24

Table 1. Image and flow properties used for artificial image generation.

The artificial two-phase images were generated by superimposing the tracer and particle images (Figure 1). Random noise was simulated by adding randomly distributed white noise with an average intensity of 7% relative to the large-particle signal, independently to every location in each two-phase image. The second image of the image-pair has an independent noise field to that of the first image.

The median filter was applied to the simulated two-phase images with a kernel size of 3×3 pixels to obtain the large-particle images. Tracer-only images were then obtained by subtracting the large-particle-only images from the two-phase images (Figure 1). The noise was removed from each tracer image by dynamic thresholding over the range 0.3 to 1. This sets all pixels below 30% of the maximum intensity to zero (black). Similarly, noise was removed from large-particle images using a threshold over the range of 0.1 to 1. Threshold ranges were optimised by varying the lower limit until the discrimination errors were minimised.

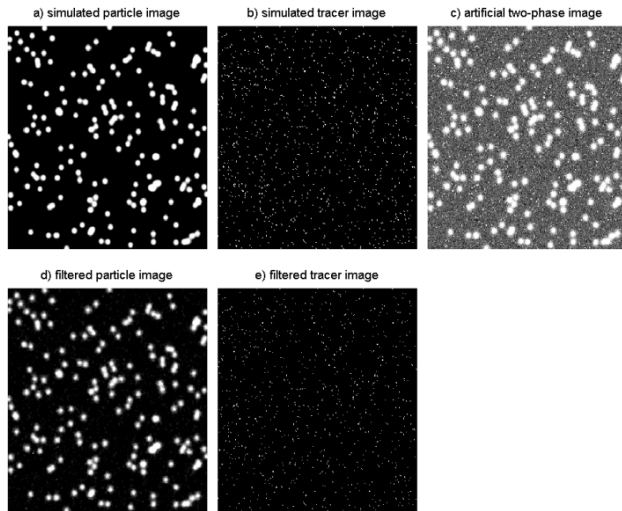


Figure 1. Examples of artificial two phase images. a) particle-only image. b) tracer-only image. c) two-phase image simulated by adding tracer-only image, particle-only image and Gaussian noise. d) regenerated large particle image from median filtering of two-phase image. e) regenerated tracer-only image by subtraction of the filtered image from the two-phase image.

PIV processing was then applied to both the original and filtered image pairs for comparison. The difference between the original and regenerated displacement fields was used to provide a matrix of absolute errors the same size as the image. The spatial mean (μ) and standard deviation (σ) of the error matrix was then used to assess performance. The simulation was repeated for each particle size (200 times) with particle mean diameters (d_p) ranging from 1 to 11 pixels (step size of 0.05). All results have been smoothed with a 10 point moving average filter.

Results

Figures 2 and 3 present μ and σ for the tracers and for the large-particles, respectively, as a function of the size of the large particles in the image, for three values of filter width (f) under the conditions shown in Table 1. This shows that, in contrast to the results of Kiger & Pan, a filter width of 3 was found to produce the smallest error for the particle displacement field (Figure 3), with no apparent difference for the error in the tracer field (Figure 2). Little difference was found in both fields when including a Gaussian mask convolution (not shown here). As a result, the mask was excluded from the simulations to reduce computational time. Kiger & Pan convolved the particle images with a sample particle (a two-dimensional Gaussian intensity profile with the same diameter as the particles) to refine the discrimination process [3, 4]. The lack of improvement found here may be attributed to the use of PIV to calculate the particle displacement field rather than PTV.

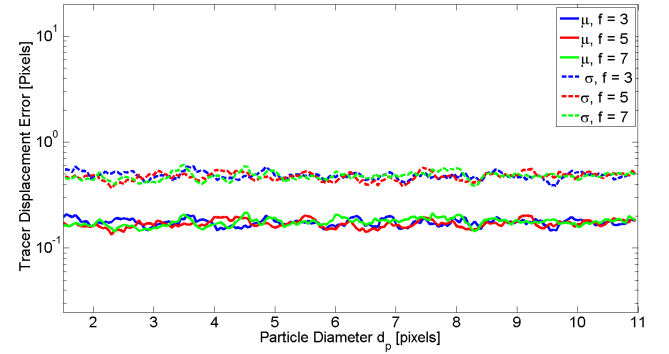


Figure 2. Spatial mean (μ) and standard deviation (σ) of the tracer displacement error field as a function of large-particle diameter (d_p) for three sizes of filter kernel size (f).

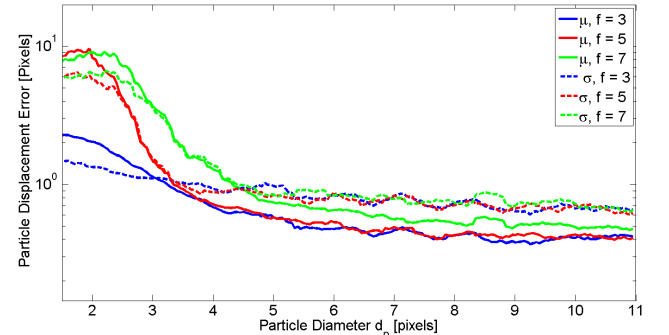


Figure 3. Spatial mean (μ) and standard deviation (σ) of the particle displacement error field as a function of large-particle diameter (d_p) for three sizes of filter kernel size (f).

The error in the particle displacement field converges to an error with μ and σ of order 1 pixel when the d_p is 5 pixels for all three examined filter sizes (Figure 3). This convergence is also present in subsequent plots.

Figure 4 and 5 show the error in the displacement of the tracer and particle, respectively, for a range of ϕ_s . Here, ϕ_s is estimated using Equation 2.

$$\phi_s = \frac{\text{particle flow rate}}{\text{fluid flow rate}} \approx \frac{\text{total volume of particles}}{\text{total volume of fluid}} = \frac{N_p d_p^3 \pi}{6h^3 LT} \quad (2)$$

Here N_p = number of particles, d_p = particle diameter [pixels] and each image is of size $h \times h$ [pixels²] and depth $LT \times h$, where LT is laser sheet thickness as a fraction of the image width. For example, 180 particles per image yields $\phi_s = 10^{-3}$ for particles with a 2 pixel (mean) d_p , and $\phi_s = 0.2$ for particles with an 11 pixel d_p .

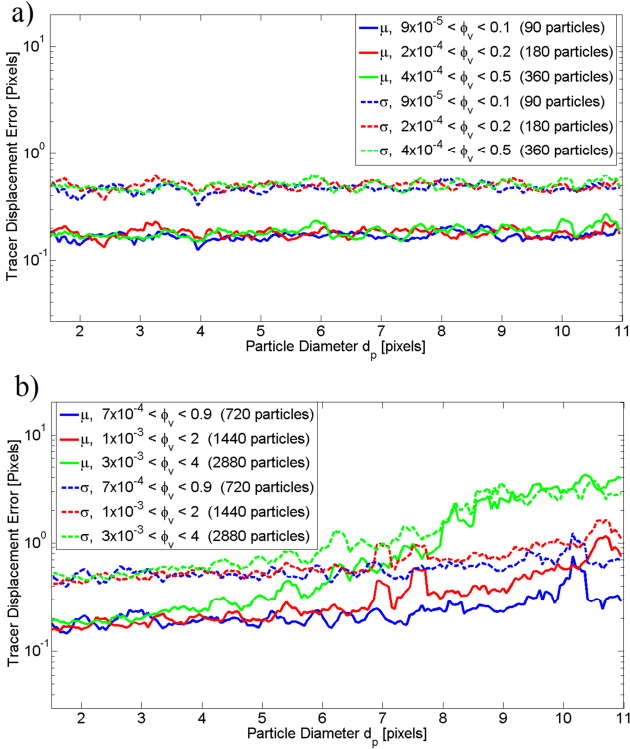


Figure 4. Spatial mean (μ) and standard deviation (σ) of the tracer displacement error field as a function of large-particle diameter (d_p) for six particle loadings.

The results show that at higher ϕ_v the error in the particle displacement field converges for smaller particle diameters (Figure 5). This may be caused by a greater number of particles providing a higher signal for PIV correlation. However, the error in the tracer field increases for particle sizes greater than 5 pixels for the 3 highest values of ϕ_v (Figure 4). This suggests that errors associated with “holes” in the regenerated data, obtained from subtracting the particles, become significant for $\phi_v \sim 0.1$. This provides an upper limit for ϕ_v for the present technique.

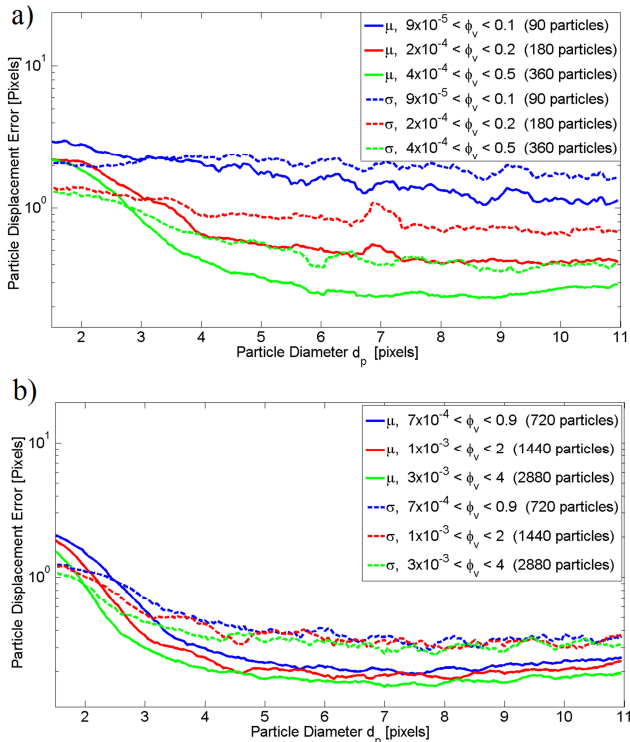


Figure 5. Spatial mean (μ) and standard deviation (σ) of the particle

displacement error field as a function of large-particle diameter (d_p) for six particle loadings.

It is important to note that the errors in the particle displacement field converge to a value of 3 pixels for $7 \times 10^{-4} < \phi_v < 0.1$. Even lower errors are produced with the 3 highest loadings (Figure 5b). Again this is probably due to a higher signal per interrogation window for PIV correlation. This suggests that the lower limit for particle loading at which the median filter technique provides accurate data may be better expressed in terms of intensity per pixel, and could be lowered by utilising PTV for the particle phase at lower ϕ_v .

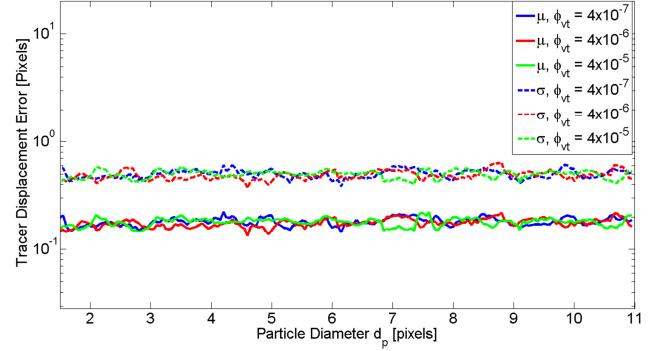


Figure 6. Spatial mean (μ) and standard deviation (σ) of the tracer displacement error field as a function of large-particle diameter (d_p) for three tracer loadings (ϕ_{tr}).

In contrast to the effect of particle loading, variation in the tracer loading (ϕ_{tr}) does not affect the filter effectiveness for the range of tracer loadings simulated (Figures 6 & 7). It is expected that at high ϕ_{tr} clusters of tracers would not be removed by the filter, causing the errors to increase. However, as the tracer particles were only 0.05 pixels in mean diameter, it is likely that the increase in ϕ_{tr} is not sufficient for these errors to become significant.

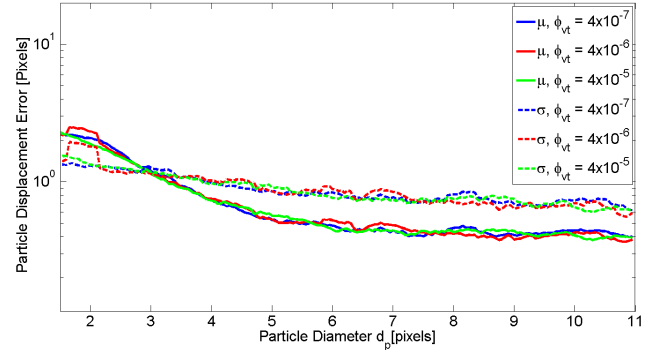


Figure 7. Spatial mean (μ) and standard deviation (σ) of the particle displacement error field as a function of large-particle diameter (d_p) for three tracer loadings (ϕ_{tr}).

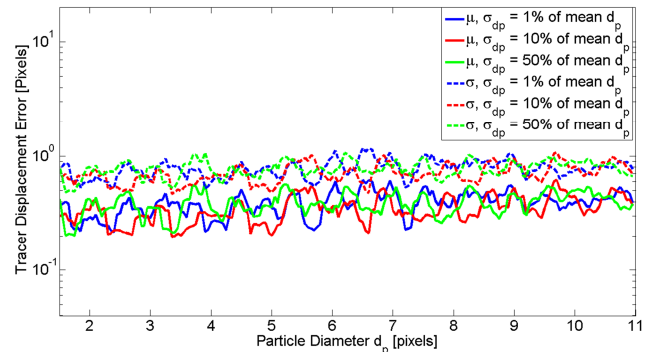


Figure 8. Spatial mean (μ) and standard deviation (σ) of the tracer

displacement error field as a function of large-particle diameter (d_p) for three standard deviations (σ_{dp}) of the d_p distribution around the mean d_p .

Since most practical two phase flows are not monodisperse, it is important to assess the influence of particle distribution on the accuracy of discrimination by the median filter technique. The particle diameters were randomly assigned using a normal distribution about the mean d_p . Figures 8 & 9 show that no discernible difference was found when the distribution had a standard deviation of 50% of the mean d_p and 1% standard deviation of the mean d_p . Therefore, the effect of particle size distribution on the accuracy of phase discrimination is negligible.

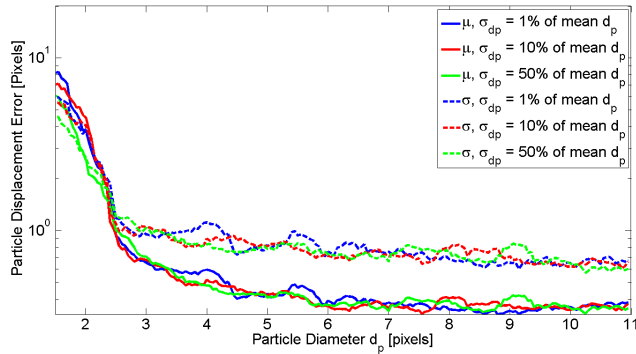


Figure 9. Spatial mean (μ) and standard deviation (σ) of the particle displacement error field as a function of large-particle diameter (d_p) for three standard deviations (σ_{dp}) of the d_p distribution around the mean d_p .

Analysis

It has been suggested that a discrimination technique provides accurate data if the absolute error in PIV displacement is less than 0.1 pixels [2-4]. In this study the absolute error typically converged to a μ of 0.5 and 0.1 pixels for the tracer and particle fields respectively, with σ typically being 1 and 0.2 pixels respectively. The relative error however, is typically 6% and 1% for μ of the particle and tracer fields, respectively. The σ of these relative errors is typically about 12% and 2%. Considering that 95.45% of errors are contained within the $\mu + 2\sigma$, relative errors within the tracer displacement field could reach values around 30%. Consequently, careful optimisation of PIV experimental settings is required for statistical measurements of the fluid phase in multiphase flows.

The effect of the large σ can somewhat be reduced by taking large sample sizes and conditionally-averaging. However systemic 'mean' errors (i.e. bias errors due to the other phase) are

much more difficult to account for during processing. Selecting a FOV such that the particle size is 3 pixels will minimise the μ (Figures 4 & 5).

Conclusions

A Monte Carlo simulation was used to assess the accuracy of a median filter technique to discriminate between the displacement fields of fluid and particles phases. This analysis has shown that:

- A filter width of 3 pixels was found to provide the best results for both tracer and particle displacement fields.
- No difference in the errors was found when using polydisperse particles with distributions with standard deviations between 1% and 50% of the mean d_p , or by varying tracer loadings (ϕ_t) over the range $4 \times 10^{-7} < \phi_t < 4 \times 10^{-5}$.
- The median filter discrimination technique achieves a mean relative displacement error of 1% and 6% for the particle and tracer fields respectively, for volumetric loadings (ϕ_v) less than 0.1, and for a resolution corresponding to a particle size (d_p) of 3 pixels.

References

- [1] Devenport, W.J., Rife, M.C., Liapis S.I. & Follin G.J., The structure and development of a wing-tip vortex, *J. Fluid Mech.*, **312**, 1996, 67–106.
- [2] Khalitov, D.A. & Longmire, E.K., Simultaneous two-phase PIV by two-parameter phase discrimination, *Exp. in Fluids*, **32**, 2002, 252-268.
- [3] Kiger, K.T. & Pan, C., Two-phase PIV for dilute solid/liquid flow, *3rd Int. Workshop on PIV*, 1999, Santa Barbara, Calif, 157-162.
- [4] Kiger, K.T. & Pan, C., PIV Technique for the Simultaneous Measurement of Dilute Two-Phase Flows, *J. Fluids. Eng. Trans. ASME*, **122**, 2000, 811-818.
- [5] Lau, T.C.W. & Nathan, G.J., New understanding of the influence of Stokes number on particle-laden jets from simultaneous planar measurements of number density and velocity', *4th ICJWS*, 2013, Nagoya, Japan.
- [6] Saffman, P.G., Ablowitz, M.J., Hinch, E.J., Ockendon, J.R. & Olver, P.J., Vortex dynamics, *Cambridge University Press*, Cambridge, 1992.